Journal of Power Sources 188 (2009) 170–176

Contents lists available at ScienceDirect

Journal of Power Sources

journal homepage: www.elsevier.com/locate/jpowsour

A reduced 1D dynamic model of a planar direct internal reforming solid oxide fuel cell for system research

Ying-Wei Kang[a,*], Jun Li[a], Guang-Yi Cao[a], Heng-Yong Tu[a], Jian Li[b], Jie Yang[b]

[a] Institute of Fuel Cell, Shanghai Jiao Tong University, Shanghai 200240, China
[b] School of Materials Science and Engineering, Huazhong University of Science and Technology, Wuhan 430074, China

ARTICLE INFO

Article history:
Received 18 July 2008
Received in revised form
20 November 2008
Accepted 20 November 2008
Available online 27 November 2008

Keywords:
SOFC
Direct internal reforming
Planar
Dynamic model
Reduced model

ABSTRACT

A reduced 1D dynamic model of a planar direct internal reforming SOFC (DIR-SOFC) is presented in this paper for system research by introducing two simplifications. The two simplification strategies employed are called Integration and Average, respectively. The present model is evaluated with a detailed 1D SOFC model, which does not introduce the two simplifications, and a lumped parameter (i.e., 0D) SOFC model. Results show that under the operating conditions investigated the accuracy of the reduced model is not significantly compromised by the two simplifications in prediction of the outlet gas flow rates and molar fractions, the outlet temperatures, and the cell voltage, while its computational time is significantly decreased by them. Moreover, it is quite simple in form. Therefore, the reduced SOFC model is attractive for system research. Compared with the lumped model, the reduced SOFC model is an improvement with regard to accuracy because it takes into account the spatially distributed nature of SOFCs to a certain extent. The discretized node number for solving the reduced model can be taken as an adjustable parameter in modeling, and is determined according to specific modeling requirements.

1. Introduction

The solid oxide fuel cell (SOFC) is attracting more and more interests as a clean and highly efficient device for power generation [1]. Since it uses an oxide ceramic material as the electrolyte, high operating temperature (typically 600–1000 °C) is required to achieve sufficient ionic conductivity. The high temperature makes it possible that the fuel reforming, when a hydrocarbon is used as the fuel, is carried out directly on the anode, giving rise to a direct internal reforming SOFC (DIR-SOFC). Moreover, the high operating temperature also produces high quality waste heat, which can be recycled by heat recovery devices or gas turbines to make combined heat and power (CHP) or hybrid systems with very high overall efficiency.

In SOFC system research, simple and accurate SOFC dynamic models are very valuable, because the model-based simulation is a valid tool for optimizing the system parameters and flowsheet, as well as for developing control strategies. In recent years, a number of distributed parameter SOFC models, ranging from 1D to 3D models, have been presented [2–4]. These models consider the spatially distributed nature of SOFC variables and the complex transport processes within the SOFC, and are useful for optimizing cell design and operating conditions. However, for SOFC system research such models have two disadvantages. First, these models are quite complex in form, and consequently are difficult to build and use. Second, solving these models using the numerical method is usually time-consuming. Up to now, what widely used in SOFC system research is the lumped parameter model (i.e., the 0D model) [5–7], which is simple in form and has an obvious advantage in computational efficiency because the internal transport processes and the spatially distributed nature of SOFCs are neglected. However, the accuracy of the lumped parameter model can be impaired for the same reasons. This is particularly true for the DIR-SOFC, which incorporates the reforming process into the cell channels. Correspondingly, the accuracy and creditability of studies by use of the lumped parameter model are also affected.

This paper will present a reduced 1D dynamic model of a planar DIR-SOFC for system research, which is simpler than the general 1D model because of introducing two simplifications. Compared with the lumped parameter model, the present model considers the spatially distributed nature of SOFCs to a certain extent, and thus is an improvement with regard to accuracy. A detailed 1D SOFC model, which does not introduce the two simplifications, and a lumped parameter SOFC model are employed to evaluate the present model. The rest of this paper is organized as follows. In Section 2, the reduced SOFC model is presented, followed by the solution method given in Section 3. In Section 4, the model evaluation is presented. Finally, conclusions are drawn in Section 5.

* Corresponding author. Tel.: +86 21 34206249; fax: +86 21 34206249.
E-mail addresses: ywkang@sjtu.edu.cn, yingwei.kang@gmail.com (Y.-W. Kang).

0378-7753/$ – see front matter © 2008 Elsevier B.V. All rights reserved.
doi:10.1016/j.jpowsour.2008.11.073

Nomenclature

$\vec{a}_{i,k}$	stoichiometric vector of species i in stream k in reactions (i)–(iv)
$\vec{a}_k$	total stoichiometric vector of stream k in reactions (i)–(iv)
A	area (m^2)
$c_{p,i}$	molar specific heat capacity of gas species i ($J\,mol^{-1}\,K^{-1}$)
$c_{p,PEN}$, $c_{p,int}$	mass specific heat capacity of the PEN and interconnect ($J\,kg^{-1}\,K^{-1}$)
C	gas molar concentration ($mol\,m^{-3}$)
E_A	activation energy ($J\,mol^{-1}$)
F	Faraday constant (=96,485 $C\,mol^{-1}$)
h	gaseous molar specific enthalpy ($J\,mol^{-1}$)
ΔH	reaction enthalpy change at the temperature of 298.15 K ($J\,mol^{-1}$)
J	average current density ($A\,m^{-2}$)
k_r	steam reforming reaction constant (=4274 $mol\,s^{-1}\,m^{-2}\,bar^{-1}$)
k_{sh}	WGS reaction constant (=1000)
K_{sh}	equilibrium constant of WGS reaction
L	cell length (m)
n	node number
n_e	number of electrons transferred per electrochemical reaction
N	molar flow rate ($mol\,s^{-1}$)
P	pressure (bar)
Q_{cond}	thermal power due to heat conduction (W)
r_j	reaction rate of reaction j ($mol\,s^{-1}\,m^{-2}$)
R	universal gas constant (=8.314 $J\,mol^{-1}\,K^{-1}$)
R_{ohm}	cell internal resistance ($\Omega\,m^2$)
S_m	molar source term ($mol\,s^{-1}\,m^{-3}$)
S_h	heat source term ($W\,m^{-3}$)
T	temperature (K)
U	cell operating voltage (V)
U_{OCV}	open circuit voltage (V)
U_0	open circuit voltage at the standard pressure (V)
W	cell width (m)
$x_{i,k}$	molar fraction of gas species i in stream k
z	spatial coordinate (m)

Greek symbols

ζ_k	number of gas species in stream k
λ	thermal conductivity ($W\,m^{-1}\,K^{-1}$)
ρ	density ($kg\,m^{-3}$)
$\Delta\tau$	computational time per time step (s)

Subscripts

a	anode
c	cathode
int	interconnect
i	gas species i
j	reaction j
k	gas stream k
PEN	PEN structure
r	steam reforming reaction
s	SOLID (including both the PEN and interconnects)
sh	WGS reaction

Superscripts

in	inlet
out	outlet
ref	reference condition (298.15 K, 1 bar)
–	spatially average value

2. Model development

Fig. 1 shows the schematic diagram of a unit planar DIR-SOFC. The unit cell consists of two interconnect plates and a tri-layer structure composed of two porous electrodes, anode and cathode, separated by a dense ion-conducting electrolyte (often referred to as the PEN). To compose an SOFC stack, repeating unit cells need to be further connected in series. The methane mixed with water steam (or their product after pre-reforming of some degree) is usually used as fuel at the anode side, and air as oxidant at the cathode side. Due to the high temperature in the SOFC, the steam reforming process directly occurs on the anode. Through electrochemical reactions the electricity is generated. All the reactions taken into account in this paper are listed in Table 1.

For the model development, several general assumptions are made as follows:

(1) Each unit cell in the SOFC stack operates identically, and there is no heat transfer between adjacent unit cells. Therefore, a unit cell can be investigated to represent the full stack performance.
(2) The SOFC is treated as a 1D plant along the gas flow direction.
(3) All gases are assumed to be ideal gas.
(4) The pressure in the gas channels is assumed to be constant.

To develop the reduced SOFC model, two simplifications are further introduced:

(a) The PEN, interconnects and gas channels are integrated together along the perpendicular direction, i.e., the SOFC is considered to have only one temperature layer.
(b) The current density distribution is considered to be uniform within the SOFC, and the cell voltage is determined by the average gas molar fractions and cell temperature.

These two simplification strategies can be called Integration and Average, respectively. By introducing Simplification (a), the complex heat transfer and gas diffusion between the SOLID (including both the PEN and interconnects) and the gas phase are neglected, and thereby the SOFC model can be greatly simplified in form. As both the electrodes and interconnects are normally good conductors, the current density actually is spatially distributed to ensure a constant operating voltage throughout the cell. To calculate the current density distribution and cell voltage, the time-consuming iterative computation is needed. By introducing Simplification (b), the cell voltage can be directly calculated by the average current density, and the iterative computation is thereby avoided. Treatments similar to Simplification (b) can also be found in Refs. [8,9].

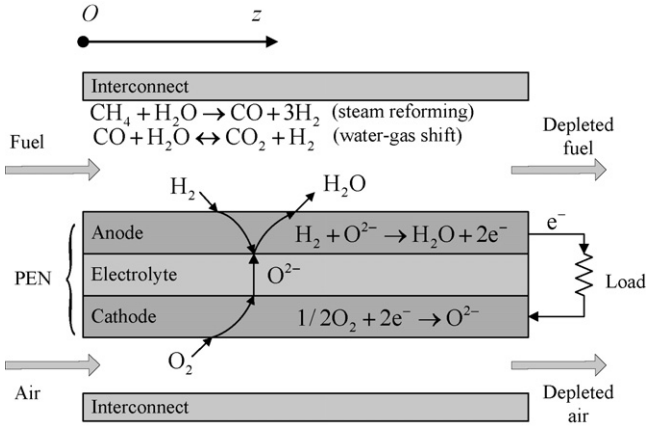

Fig. 1. Schematic diagram of a unit planar DIR-SOFC.

Table 1
Reactions considered in this paper.

Reaction name	Reaction equation	Location	ΔH (J mol^{-1})
Methane steam reforming	$CH_4 + H_2O \rightarrow CO + 3H_2$ (i)	Anode gas channels	206,100
Water-gas shift (WGS)	$CO + H_2O \leftrightarrow CO_2 + H_2$ (ii)	Anode gas channels	−41,150
Hydrogen oxidation	$H_2 + O^{2-} \rightarrow H_2O + 2e^-$ (iii)	Anode	–
Oxygen reduction	$(1/2)O_2 + 2e^- \rightarrow O^{2-}$ (iv)	Cathode	–
Overall electrochemical reaction	$H_2 + (1/2)O_2 \rightarrow H_2O$ (v)	–	−241,800

By applying above assumptions and simplifications, the reduced SOFC model can be developed based on mass and energy balances, and electrochemical principles. Fig. 2 gives the schematic representation of the reduced model.

2.1. Mass balances

There are five gas species in the anode channels, i.e., CH_4, H_2O, H_2, CO and CO_2, and two gas species in the cathode channels, i.e., O_2 and N_2. By applying the molar balance to species i in the anode channels, the following molar fraction dynamic equation is obtained:

$$\frac{\partial(C_a x_{i,a})}{\partial t} + \frac{1}{A_a}\frac{\partial(N_a x_{i,a})}{\partial z} = S_{m,i,a}, \quad i \in \{CH_4, H_2O, H_2, CO, CO_2\}, \tag{1}$$

where C_a is the total molar concentration of anode gases, $x_{i,a}$ the molar fraction of species i in the anode gas stream, A_a the total section area of anode channels, N_a the molar flow rate of the anode gas stream, and $S_{m,i,a}$ the molar source term of species i in anode channels.

For the gases in the anode channels, the following total molar balance equation can also be built:

$$\frac{\partial C_a}{\partial t} + \frac{1}{A_a}\frac{\partial N_a}{\partial z} = S_{m,a}, \tag{2}$$

where $S_{m,a}$ is the total molar source term of the gases in anode channels. Neglecting the total molar concentration transient of gases in anode channels (i.e., the first term on the left hand side of Eq. (2)), we have the following ordinary differential equation:

$$\frac{1}{A_a}\frac{\partial N_a}{\partial z} = S_{m,a} \tag{3}$$

Similarly, for the gases in the cathode channels we have:

$$\frac{\partial(C_c x_{i,c})}{\partial t} + \frac{1}{A_c}\frac{\partial(N_c x_{i,c})}{\partial z} = S_{m,i,c}, \quad i \in \{O_2, N_2\}, \tag{4}$$

and

$$\frac{1}{A_c}\frac{\partial N_c}{\partial z} = S_{m,c}. \tag{5}$$

The molar source terms of individual gas species, i.e., $S_{m,i,a}$ and $S_{m,i,c}$, and the total molar source terms, i.e., $S_{m,a}$ and $S_{m,c}$, are related to the rates of reactions in the SOFC. Defining a vector $\vec{r} = [\, r_i \quad r_{ii} \quad r_{iii} \quad r_{iv} \,]^T$ to represent the rates of reactions (i)–(iv), these molar source terms can be expressed as

$$S_{m,i,k} = \vec{a}_{i,k}^T \mathrm{diag}\left(\frac{W}{A_a}, \frac{W}{A_a}, \frac{W}{A_a}, \frac{W}{A_c}\right)\vec{r}, \tag{6}$$

and

$$S_{m,k} = \vec{a}_k^T \mathrm{diag}\left(\frac{W}{A_a}, \frac{W}{A_a}, \frac{W}{A_a}, \frac{W}{A_c}\right)\vec{r}, \quad k \in \{a, c\}, \tag{7}$$

where $\vec{a}_{i,k} \in R^4$ is the stoichiometric vector of species i in gas stream k in reactions (i)–(iv), $\vec{a}_k \in R^4$ the total stoichiometric vector of gas stream k in reactions (i)–(iv), and W the cell width.

The reaction rates are calculated as follows [2,4,10]:

$$r_i = k_r P_a x_{CH_4,a} \exp\left(\frac{-E_{A,r}}{RT}\right), \tag{8}$$

$$r_{ii} = k_{sh} P_a x_{CO,a}\left(1 - \frac{x_{CO_2,a} x_{H_2,a} / x_{CO,a} x_{H_2O,a}}{K_{sh}}\right), \tag{9}$$

$$r_{iii} = r_{iv} = r_v = \frac{J}{2F}, \tag{10}$$

where $E_{A,r}$ is the activation energy of the steam reforming reaction, T the SOFC temperature, J the average current density, and K_{sh} the equilibrium constant of the WGS reaction with $K_{sh} = \exp(4276/T - 3.961)$ [11].

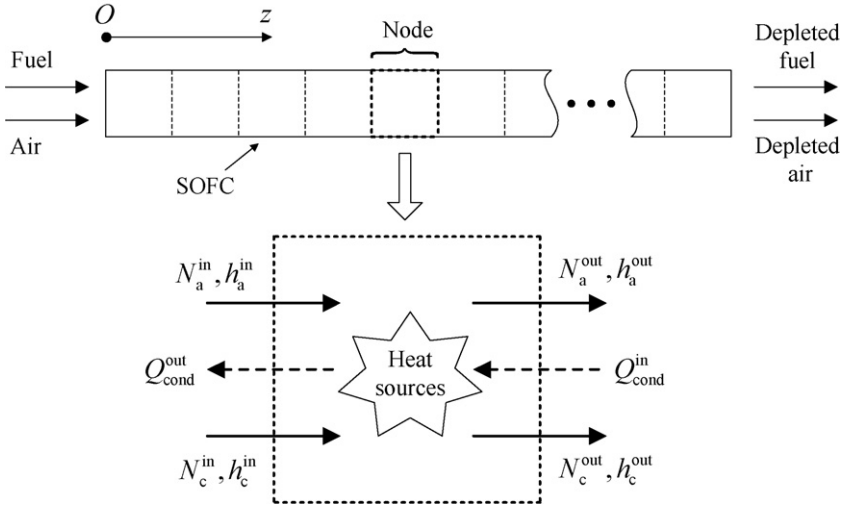

Fig. 2. Schematic representation of the reduced model.

2.2. Energy balance

According to Simplification (a), the energy balance equation for the SOFC can be written as

$$\frac{A_{\mathrm{PEN}}\rho_{\mathrm{PEN}}c_{p,\mathrm{PEN}} + A_{\mathrm{int}}\rho_{\mathrm{int}}c_{p,\mathrm{int}}}{A}\frac{\partial T}{\partial t} + \frac{A_{\mathrm{a}}}{A}\frac{\partial(C_{\mathrm{a}}h_{\mathrm{a}})}{\partial t} + \frac{A_{\mathrm{c}}}{A}\frac{\partial(C_{\mathrm{c}}h_{\mathrm{c}})}{\partial t} + \frac{1}{A}\frac{\partial(N_{\mathrm{a}}h_{\mathrm{a}})}{\partial z} + \frac{1}{A}\frac{\partial(N_{\mathrm{c}}h_{\mathrm{c}})}{\partial z} = \frac{A_{\mathrm{PEN}}\lambda_{\mathrm{PEN}} + A_{\mathrm{int}}\lambda_{\mathrm{int}}}{A}\frac{\partial^2 T}{\partial z^2} + S_{\mathrm{h}}, \quad (11)$$

where A is the cell section area, A_{PEN} (A_{int}), ρ_{PEN} (ρ_{int}), $c_{p,\mathrm{PEN}}$ ($c_{p,\mathrm{int}}$), and λ_{PEN} (λ_{int}) the section area, density, mass specific heat capacity, and thermal conductivity of the PEN (interconnect), respectively, h_{a} (h_{c}) the molar specific enthalpy of the anode (cathode) gas mixture, and S_{h} the heat source term.

The first term on the left-hand side of Eq. (11) represents the rate of energy accumulation in the SOLID; the second and third terms represent those in the anode and cathode gas phases, respectively, and can be neglected because the heat capacity of the gas phases is far smaller than that of the SOLID; the forth and fifth terms represent the enthalpy fluxes due to gas convection in the anode and cathode channels, respectively. The first term on the right-hand side of Eq. (11) represents the heat conduction in the SOLID modeled by Fourier's law of conduction.

The heat source term, S_{h}, is expressed as

$$S_{\mathrm{h}} = \frac{(-r_{\mathrm{i}}\,\Delta H_{\mathrm{i}} - r_{\mathrm{ii}}\,\Delta H_{\mathrm{ii}} - r_{\mathrm{v}}\,\Delta H_{\mathrm{v}} - UJ)\cdot W}{A}, \quad (12)$$

where ΔH_j is the enthalpy change of reaction j at the temperature of 298.15 K, and U the cell operating voltage. In Eq. (12), Simplification (b) has been employed (i.e., the uniform current density distribution is assumed), and thereby the electrochemically generated heat is also uniformly distributed in the SOFC.

The specific enthalpy of the gas mixture (i.e., h_{a} and h_{c} in Eq. (11)) is calculated as a function of the local gas molar fraction by

$$h_k = \sum_{i=1}^{\zeta_k} x_{i,k}h_i, \quad k \in \{\mathrm{a}, \mathrm{c}\}. \quad (13)$$

The specific enthalpy of gas species i at the temperature of T, $h_i(T)$, is calculated by

$$h_i(T) = \int_{T^{\mathrm{ref}}}^{T} c_{p,i}(T)\ \mathrm{d}T, \quad (14)$$

with $T^{\mathrm{ref}} = 298.15$ K, where $c_{p,i}$ is the molar specific heat capacity of species i and is expressed as a third degree polynomial function of T [12].

2.3. Electrochemical model

In this model, the average current density, which reflects the external load demand, is specified, and the cell operating voltage is then determined. The cell operating voltage is calculated by subtracting various irreversible overpotentials from the reversible open circuit voltage. According to Simplification (b), the average cell temperature and gas molar fractions are used in the calculation of the reversible open circuit voltage and various irreversible overpotentials.

The reversible open circuit voltage is given by the Nernst equation:

$$U_{\mathrm{OCV}} = U_0(\bar{T}) + \frac{R\bar{T}}{2F}\ \ln\left[\frac{\bar{x}_{\mathrm{H_2,a}}\bar{x}_{\mathrm{O_2,c}}^{0.5}P_{\mathrm{c}}^{0.5}}{\bar{x}_{\mathrm{H_2O,a}}}\right], \quad (15)$$

with $U_0(\bar{T}) = 1.2723 - 2.7645\times10^{-4}\bar{T}$, where $U_0(\bar{T})$ is the reversible open circuit voltage at the temperature of $\bar{T}$ and the standard pressure [11].

The cell operating voltage is calculated by

$$U = U_{\mathrm{OCV}} - JR_{\mathrm{ohm}}(\bar{T}) - \frac{2R\bar{T}}{n_{\mathrm{e}}F}\sinh^{-1}\left(\frac{J}{2j_{0,\mathrm{a}}}\right) - \frac{2R\bar{T}}{n_{\mathrm{e}}F}\sinh^{-1}\left(\frac{J}{2j_{0,\mathrm{c}}}\right) + \frac{R\bar{T}}{2F}\ \ln\left(1-\frac{J}{j_{\mathrm{L}}}\right). \quad (16)$$

The second to fifth terms on the right-hand side of Eq. (16) represent the ohmic, anode and cathode activation, and concentration overpotentials, respectively. In this equation, R_{ohm} is the internal resistance of the cell, which is a function of the temperature and is calculated from the conductivity of the individual layers [4]; $j_{0,\mathrm{a}}$ and $j_{0,\mathrm{c}}$ are the anode and cathode exchange current densities, respectively, and are determined by the method of Ref. [13]; j_{L} is the limiting current density at which the fuel is used up at a rate equal to its maximum supply speed in the electrode and the cell voltage falls rapidly to zero.

2.4. Boundary conditions

The two ends of the SOLID are both assumed to be insulated. The inlet boundary conditions of gas streams are specified by the inlet gas conditions including the anode and cathode gas temperatures, molar fractions and flow rates.

3. Solution method

Eqs. (1), and (3)–(16), and the relevant boundary conditions compose an equation system, which can be solved using the finite volume method [14]. The SOFC domain is divided into n uniform nodes along the cell length direction, with the grid points located at the centers of the nodes. The convection terms in Eqs. (1) and (4) are discretized using the first-order upwind scheme, and the diffusion term in Eq. (11) using the second-order central difference scheme [14]. As the equation system is stiff, its transient terms are integrated using the stiff solver ode23s provided by MATLAB R2006a.

In each time step, according to the specified average current density the electrochemical model is first solved to obtain the cell voltage. Afterwards, the molar source terms (Eqs. (6) and (7)) and heat source term (Eq. (12)) are calculated. Next, the molar flow rates N_{a} and N_{c} are calculated from Eqs. (3) and (5). Then, the state variables are updated from Eqs. (1), (4) and (11). According to the solution strategy presented, a MATLAB code is designed to solve this model.

4. Model evaluation

The reduced SOFC model (R.M.) is evaluated with a detailed model (D.M.) [15] and a lumped parameter model (L.M.). The D.M. is also a 1D SOFC model as the R.M. but without introducing Simplifications (a) and (b). In the D.M., the SOFC is divided into three temperature layers, i.e., the fuel stream in anode channels, the air stream in cathode channels and the SOLID. The convective heat transfer and the gas diffusion between the SOLID and the gas channels are considered comprehensively. Moreover, the Newton–Raphson iteration is employed to calculate the current density distribution and cell voltage. The L.M. is a 0D SOFC model as given in Ref. [7], which neglects the spatial variations of SOFC variables, such as the current density, temperatures and gas compositions, and is built by applying mass and energy balances to

Table 2
SOFC specifications.

Dimensions of the cell	
Cell length (m)	0.1
Cell width (m)	0.1
Anode thickness (m)	500×10^{-6}
Cathode thickness (m)	50×10^{-6}
Electrolyte thickness (m)	20×10^{-6}
Interconnect thickness (m)	500×10^{-6}
Fuel channel height (m)	1.0×10^{-3}
Air channel height (m)	1.0×10^{-3}
Material properties of the cell	
Anode electrical conductivity (Ω^{-1} m^{-1})	8.0×10^{4}
Cathode electrical conductivity (Ω^{-1} m^{-1})	8.0×10^{3}
Electrolyte ionic conductivity (Ω^{-1} m^{-1})	$3.34 \times 10^{4} \exp(-10{,}300/T)$
PEN density (kg m^{-3})	5900
PEN heat capacity (J kg^{-1} K^{-1})	500
PEN thermal conductivity (W m^{-1} K^{-1})	2
Interconnect density (kg m^{-3})	8000
Interconnect heat capacity (J kg^{-1} K^{-1})	500
Interconnect thermal conductivity (W m^{-1} K^{-1})	25
Activation and concentration overpotential data	
Activation energy of anode (J mol^{-1})	140,000
Activation energy of cathode (J mol^{-1})	137,000
Pre-exponential coefficient for anode (A m^{-2})	8.0×10^{10}
Pre-exponential coefficient for cathode (A m^{-2})	1.5×10^{10}
Limiting current density (A m^{-2})	12,000

the global SOFC domain. The L.M. therefore can predict a single SOFC temperature. The transient terms of the D.M. and the L.M. are also integrated using ode23s. A co-flow planar anode-supported DIR-SOFC is adopted in the evaluation. The specifications of the SOFC are listed in Table 2. All the computations are performed on an AMD Sempron™ 1.6 GHz computer with 512 MB RAM.

The steady-state operating conditions used for model evaluation are listed in Table 3, where Case 1 is the nominal operating condition and Cases 2–5 represent the operating conditions of high load current, high fuel utilization, low air ratio, and high gas inlet temperature difference, respectively. The steady-state performance of the D.M. with 100 nodes, the L.M., and the R.M. with 100 nodes under these operating conditions are listed in Tables 4–6, respectively. Among these models, the D.M. with 100 nodes is considered to be the most accurate one because the least simplifications and 100 discretized nodes are employed. The terms compared involve anode and cathode outlet gas molar fractions, molar flow rates, and temperatures, average and outlet SOLID temperatures, cell voltage, and computational time per time step.

From Tables 4 and 5, the L.M. and the D.M. can first be compared to show the performance of the lumped model. It can be seen that the L.M. achieves the same prediction results as the D.M. in the cathode outlet gas molar flow rate and molar fractions. However, there exist noticeable prediction errors in the anode outlet gas molar flow rate and molar fractions, particularly the outlet molar fractions of CH_4, H_2, and CO. This is disadvantageous for system research, because in an SOFC system the anode exit gases are usually burned for energy recycling. Moreover, it can be found that the temperature predicted by the L.M. (e.g., 1129.3 K for Case 1) is close to the outlet SOLID temperature (e.g., 1121.8 K for Case 1) rather than the average SOLID temperature (e.g., 1037.3 K for Case 1) predicted by the D.M. Therefore, the temperature predicted by the L.M. should be viewed as the outlet temperature for a co-flow SOFC. It is worth noting that the prediction errors of Case 3 in the outlet temperatures are all beyond 30 K and that in the cell voltage approximates 0.1 V. This indicates that the prediction accuracy of the L.M. significantly decreases at high fuel utilization level.

Table 3
Steady-state operating conditions used for model evaluation.

	Case number				
	1	2	3	4	5
Average current density (A m^{-2})	5000	6000	5000	5000	5000
Fuel utilization	0.8	0.8	0.9	0.8	0.8
Air ratio	7.5	7.5	7.5	5.5	7.5
Inlet fuel temperature (K)	1023	1023	1023	1023	1048
Inlet air temperature (K)	1023	1023	1023	1023	998
Inlet gas composition	Fuel: CH_4 0.33, H_2O 0.67; air: O_2 0.21, N_2 0.79				
Operating pressure (bar)	1				

Table 4
Steady-state performance of the D.M. with 100 nodes.

	Case 1	Case 2	Case 3	Case 4	Case 5
$x^{out}_{CH_4,a}$	6.0400e−5	1.4616e−4	6.0926e−6	4.0926e−5	1.5841e−4
$x^{out}_{H_2O,a}$	0.6772	0.6785	0.7398	0.6793	0.6767
$x^{out}_{H_2,a}$	0.1239	0.1227	0.0614	0.1219	0.1244
$x^{out}_{CO,a}$	0.0349	0.0358	0.0181	0.0370	0.0340
$x^{out}_{CO_2,a}$	0.1639	0.1629	0.1807	0.1618	0.1647
N^{out}_a (mol s^{-1})	4.0726e−4	4.8863e−4	3.6205e−4	4.0728e−4	4.0718e−4
$x^{out}_{O_2,c}$	0.1872	0.1872	0.1872	0.1786	0.1872
$x^{out}_{N_2,c}$	0.8128	0.8128	0.8128	0.8214	0.8128
N^{out}_c (mol s^{-1})	4.4974e−3	5.3968e−3	4.4974e−3	3.2635e−3	4.4974e−3
$\bar{T}_s$ (K)	1037.3	1043.8	1053.3	1037.4	1021.1
T^{out}_s (K)	1121.8	1135.2	1133.9	1149.2	1112.0
T^{out}_a (K)	1122.5	1136.0	1134.4	1150.0	1112.7
T^{out}_c (K)	1116.6	1127.0	1130.3	1145.0	1106.0
U (V)	0.6582	0.6238	0.6599	0.6626	0.6252
$\Delta\tau$ (s)	23.6102				

Table 5
Steady-state performance of the L.M.

	Case 1	Case 2	Case 3	Case 4	Case 5
$x^{out}_{CH_4,a}$	0.0111	0.0123	0.0077	0.0094	0.0123
$x^{out}_{H_2O,a}$	0.7046	0.7081	0.7603	0.7019	0.7067
$x^{out}_{H_2,a}$	0.0922	0.0882	0.0379	0.0956	0.0896
$x^{out}_{CO,a}$	0.0259	0.0254	0.0121	0.0287	0.0241
$x^{out}_{CO_2,a}$	0.1662	0.1660	0.1820	0.1644	0.1673
N^{out}_a (mol s^{-1})	3.9845e−4	4.7700e−4	3.5657e−4	3.9977e−4	3.9752e−4
$x^{out}_{O_2,c}$	0.1872	0.1872	0.1872	0.1786	0.1872
$x^{out}_{N_2,c}$	0.8128	0.8128	0.8128	0.8214	0.8128
N^{out}_c (mol s^{-1})	4.4974e−3	5.3968e−3	4.4974e−3	3.2635e−3	4.4974e−3
$\bar{T}_s$ (K)	1129.3	1138.7	1165.1	1152.1	1115.5
T^{out}_s (K)	1129.3 (7.5)[a]	1138.7 (3.5)	1165.1 (31.2)	1152.1 (2.9)	1115.5 (3.5)
T^{out}_a (K)	1129.3 (6.8)	1138.7 (2.7)	1165.1 (30.7)	1152.1 (2.1)	1115.5 (2.8)
T^{out}_c (K)	1129.3 (12.7)	1138.7 (11.7)	1165.1 (34.8)	1152.1 (7.1)	1115.5 (9.5)
U (V)	0.6405 (−0.0177)	0.6124 (−0.0114)	0.5632 (−0.096)	0.6648 (0.0022)	0.6200 (−0.0052)
$\Delta\tau$ (s)	0.0137				

[a] The value in parenthesis is the prediction error compared with the D.M.

Table 6
Steady-state performance of the R.M. with 100 nodes.

	Case 1	Case 2	Case 3	Case 4	Case 5
$x^{out}_{CH_4,a}$	3.7721e−5	9.3690e−5	6.6218e−6	1.6553e−5	8.7239e−5
$x^{out}_{H_2O,a}$	0.6767	0.6777	0.7396	0.6785	0.6760
$x^{out}_{H_2,a}$	0.1245	0.1235	0.0616	0.1227	0.1252
$x^{out}_{CO,a}$	0.0344	0.0352	0.0179	0.0363	0.0336
$x^{out}_{CO_2,a}$	0.1644	0.1635	0.1809	0.1625	0.1652
N^{out}_a (mol s^{-1})	4.0728e−4	4.8868e−4	3.6205e−4	4.0730e−4	4.0724e−4
$x^{out}_{O_2,c}$	0.1872	0.1872	0.1872	0.1786	0.1872
$x^{out}_{N_2,c}$	0.8128	0.8128	0.8128	0.8214	0.8128
N^{out}_c (mol s^{-1})	4.4974e−3	5.3968e−3	4.4974e−3	3.2635e−3	4.4974e−3
$\bar{T}_s$ (K)	1041.1 (3.8)	1047.4 (3.6)	1050.0 (−3.3)	1049.0 (11.6)	1028.1 (7.0)
T^{out}_s (K)	1116.3 (−5.5)	1127.0 (−8.2)	1128.2 (−5.7)	1141.0 (−8.2)	1105.6 (−6.4)
T^{out}_a (K)	1116.3 (−6.2)	1127.0 (−9.0)	1128.2 (−6.2)	1141.0 (−9.0)	1105.6 (−7.1)
T^{out}_c (K)	1116.3 (−0.3)	1127.0 (0.0)	1128.2 (−2.1)	1141.0 (−4.0)	1105.6 (−0.4)
U (V)	0.6614 (0.0032)	0.6268 (0.0030)	0.6678 (0.0079)	0.6740 (0.0114)	0.6287 (0.0035)
$\Delta\tau$ (s)	3.4396				

Then, from Tables 4 and 6, the R.M. and the D.M. can be compared to show the performance of the reduced model. It can be found that the R.M. also achieves the same prediction results as the D.M. in the cathode outlet gas molar flow rate and molar fractions. Moreover, there is very little difference in the anode outlet gas molar flow rate and molar fractions predicted by the two models. This is an improvement compared with the L.M. The outlet temperatures predicted by the R.M. are generally lower than those predicted by the D.M. This is because introducing the simplification of uniform current density distribution flats the temperature distributions. As a whole, the prediction errors in the average and outlet temperatures and the cell voltage under different operating conditions are modest. The prediction errors in these variables slightly increase in the low air ratio case (i.e., Case 4) and the high gas inlet temperature difference case (i.e., Case 5). These results indicate that the R.M.'s accuracy is not significantly compromised by the two simplifications under the operating conditions investigated. It can also be found that the computational time of the R.M. is significantly lower than that of the D.M. due to employing the two simplifications.

To further verify the dynamic performance of the reduced model, Fig. 3 shows the dynamic responses of the D.M. with 100 nodes, the L.M., and the R.M. with 100 nodes to the applied average current density disturbances. It can be found that these models exhibit similar dynamics in the outlet SOLID

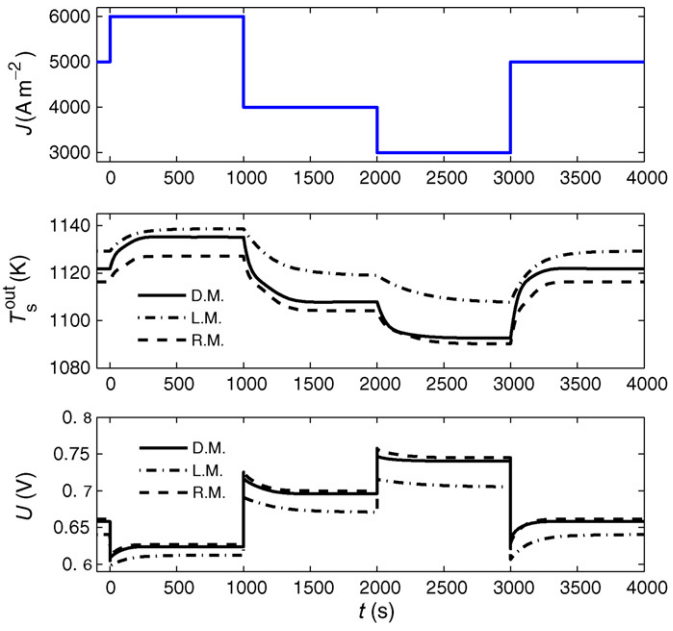

Fig. 3. Comparison of dynamic responses of the D.M. with 100 nodes, the L.M., and the R.M. with 100 nodes to applied load current disturbances.

temperature and the cell voltage for the applied load current disturbances.

When the node number of the R.M. is reduced to one, it will have the same equation form as the L.M. Therefore, the L.M. can be viewed as the R.M. with one node. The R.M. approximates the spatially distributed nature of SOFCs along the gas flow direction by connecting a series of scale-down L.M.s with consideration of the heat conduction and gas transport between adjacent nodes. Therefore, the node number can be taken as an adjustable parameter in modeling, and is determined according to specific modeling requirements for accuracy and computational time.

5. Conclusions

A reduced 1D dynamic model of a planar DIR-SOFC has been presented in this paper for system research by introducing two simplifications. A detailed 1D SOFC model without introducing the two simplifications and a lumped parameter SOFC model are employed to evaluate the present model for a co-flow planar anode-supported DIR-SOFC. From the model evaluation results, several conclusions can be drawn as follows:

(1) Under the operating conditions investigated, the accuracy of the reduced model is not significantly compromised by the two simplifications in prediction of the outlet gas flow rates and molar fractions, the outlet temperatures, and the cell voltage, while its computational time is significantly decreased by them. More noticeable predictions errors are possible under extreme operating conditions. Moreover, it is quite simple in form. Therefore, the reduced model provides a choice of modeling for SOFC system research.
(2) Compared with the lumped model, the reduced model is an improvement with regard to accuracy, because the reduced model can be viewed as a series of scale-down lumped models, which are connected to approximate the spatially distributed nature of SOFCs along the gas flow direction.
(3) The discretized node number for solving the reduced model can be taken as an adjustable parameter in modeling, and is determined according to specific modeling requirements for accuracy and computational time.

In the future, the reduced SOFC model will be used for system optimization and control design.

Acknowledgement

The research work is supported by the National High Technology Research and Development Program of China (No. 2006AA05Z148).

References

[1] S.C. Singhal, K. Kendall (Eds.), High Temperature Solid Oxide Fuel Cells: Fundamentals, Design and Applications, Elsevier Advanced Technology, Oxford, 2003.
[2] E. Achenbach, J. Power Sources 49 (1994) 333–348.
[3] L. Petruzzi, S. Cocchi, F. Fineschi, J. Power Sources 118 (2003) 96–107.
[4] P. Aguiar, C.S. Adjiman, N.P. Brandon, J. Power Sources 138 (2004) 120–136.
[5] A.M. Murshed, B. Huang, K. Nandakumar, J. Power Sources 163 (2007) 830–845.
[6] R. Kandepu, L. Imsland, B.A. Foss, C. Stiller, B. Thorud, O. Bolland, Energy 32 (2007) 406–417.
[7] Y.-W. Kang, J. Li, G.-Y. Cao, H.-Y. Tu, J. Li, J. Yang, J. Power Sources 179 (2008) 683–692.
[8] D.F. Cheddie, N.D.H. Munroe, J. Power Sources 171 (2007) 634–643.
[9] X. Zhang, J. Li, G. Li, Z. Feng, J. Power Sources 160 (2006) 258–267.
[10] E. Achenbach, E. Riensche, J. Power Sources 52 (1994) 283–288.
[11] S. Campanari, P. Iora, J. Power Sources 132 (2004) 113–126.
[12] B.G. Kyle, Chemical and Process Thermodynamics, Prentice Hall, Englewood Cliffs, 1984.
[13] P. Costamagna, K. Honegger, J. Electrochem. Soc. 145 (1998) 3995–4007.
[14] S.V. Patankar, Numerical Heat Transfer and Fluid Flow, Hemisphere, Washington, 1980.
[15] Y.-W. Kang, J. Li, G.-Y. Cao, H.-Y. Tu, J. Li, J. Yang, Chin. J. Chem. Eng., in press.